Cell Reports, Volume *44*

Supplemental information

YAP1 is a key regulator of EWS::FLI1-dependent malignant transformation upon IGF-1-mediated reprogramming of bone mesenchymal stem cells

Rahil Noorizadeh, Barbara Sax, Tahereh Javaheri, Branka Radic-Sarikas, Valerie Fock, Veveeyan Suresh, Maximilian Kauer, Aleksandr Bykov, Danijela Kurija, Michaela Schlederer, Lukas Kenner, Gerhard Weber, Wolfgang Mikulits, Florian Halbritter, Richard Moriggl, and Heinrich Kovar

Figure S1

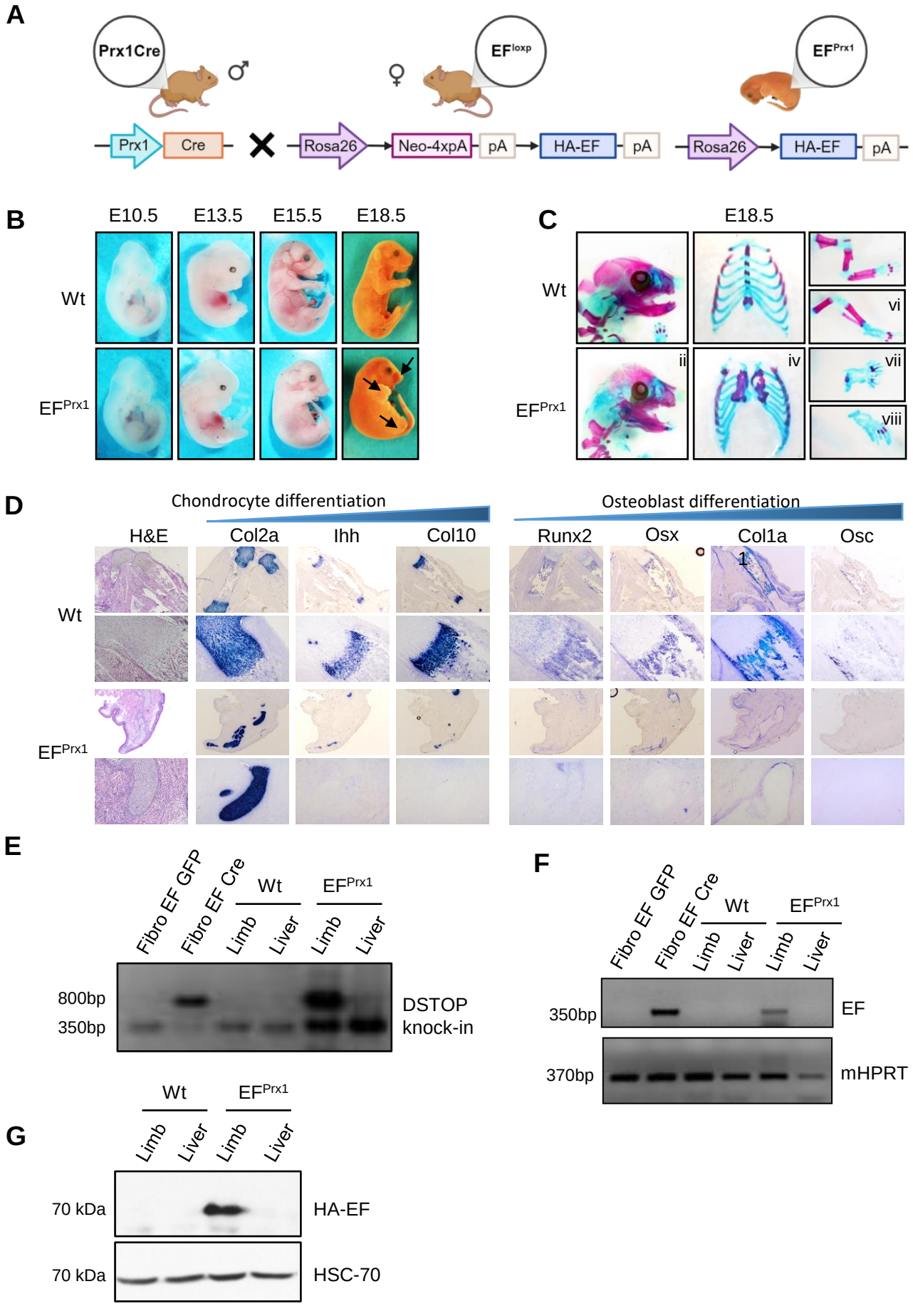
A
Prx1Cre
♂
♀
EFloxp
EFPrx1
Prx1
Cre
Rosa26
Neo-4xpA
pA
HA-EF
pA
Rosa26
HA-EF
pA
B
E10.5
E13.5
E15.5
E18.5
Wt
EFPrx1
C
E18.5
Wt
EFPrx1
ii
iv
vi
vii
viii
D
Chondrocyte differentiation
Osteoblast differentiation
H&E
Col2a
Ihh
Col10
Runx2
Osx
Col1a
Osc
Wt
EFPrx1
25x
100x
25x
100x
E
Fibro EF GFP
Fibro EF Cre
Wt
EFPrx1
Limb
Liver
Limb
Liver
800bp
350bp
DSTOP
knock-in
F
Fibro EF GFP
Fibro EF Cre
Wt
EFPrx1
Limb
Liver
Limb
Liver
350bp
EF
370bp
mHPRT
G
Wt
EFPrx1
Limb
Liver
Limb
Liver
70 kDa
HA-EF
70 kDa
HSC-70

Figure S1. Early EF expression in MSCLC during embryogenesis causes endochondral *bone formation* arrest.

(A) Schematic drawing of EF^{Prx1} mice generation by crossing Prx1-Cre mice with Rosa26 loxP-STOP-loxP-HA-EF (EF^{loxp}) mice. Black arrows: loxP sites. Hemagglutinin tag: HA, EWS::FLI1: EF. **(B)** EF^{Prx1} mouse embryos exhibit multiple abnormalities of the limbs and the cranium (blue dashed arrows). **(C)** Skeletal preparations and analysis with Alcian Blue/Alizarin Red staining of E18.5 Wt and EF^{Prx1} embryos. Blue staining marks cartilage elements, whereas pink color indicates calcified bone. EF^{Prx1} embryos had defects in the development of craniofacial (i,ii), the sternum (iii, iv), forelimbs (v, vii), and hindlimbs (vi,viii). **(D)** Hematoxylin and Eosin (H&E) stains of the E18.5 limb structures (left) revealed a well-organized bone tissue context with distinct cell layers till the epidermis, while the limb structure of EF^{Prx1} embryos appeared completely disorganized. Endochondral bone formation is tightly linked to chondrocyte differentiation. Thus, we labelled the cartilage elements of the limb anlage of Wt and EF^{Prx1} embryos with different markers by non-radioactive *in situ* hybridisation to map distinct differentiation zones. From left to right, the markers are displayed according to their temporal expression sequence during bone maturation as indicated on top of the figure. In the Wt mouse, the resting zones on top and bottom of longitudinal bone development are marked by expression of *Col2a1* and *Indian hedgehog* (*Ihh*) specific for the pre-hypertrophic chondrocyte stage, and *Col10a1* marking hypertrophic chondrocyte zones. In contrast to the wt embryos, the limb anlage of EF^{Prx1} mutant mice lack an organized longitudinal bone structure with loss of expression of all osteoblast markers. While there was a clear labelling of different endochondral bone formation zones in wt limbs, we saw mis localized staining signals in EF^{Prx1} embryo limbs, that only display *Col2a1* expression and patchy *Ihh in situ* hybridization signals in some small elements, consistent with early chondrocytic differentiation arrest in bone development. Results are displayed in two magnifications (25x and 100x). **(E)** Analysis of genomic DNA of wild type (Wt) and EF^{Prx1} mice (E17.5) for deletion of STOP-cassette (DSTOP) with a PCR strategy. **(F)** Detection of EF expression from reverse transcribed cDNA with EF-specific primers. mHPRT was used as an internal control. Fibro EF GFP or Cre: fibroblasts isolated from EF mice lentivirally transduced with an expression construct encoding GFP or Cre recombinase served as negative and positive controls. **(G)** The presence of EF protein in EF^{Prx1} limbs was verified by immunoblot analysis using an antibody specific for the HA-tag. HSC-70 was used as a loading control.

Figure S2

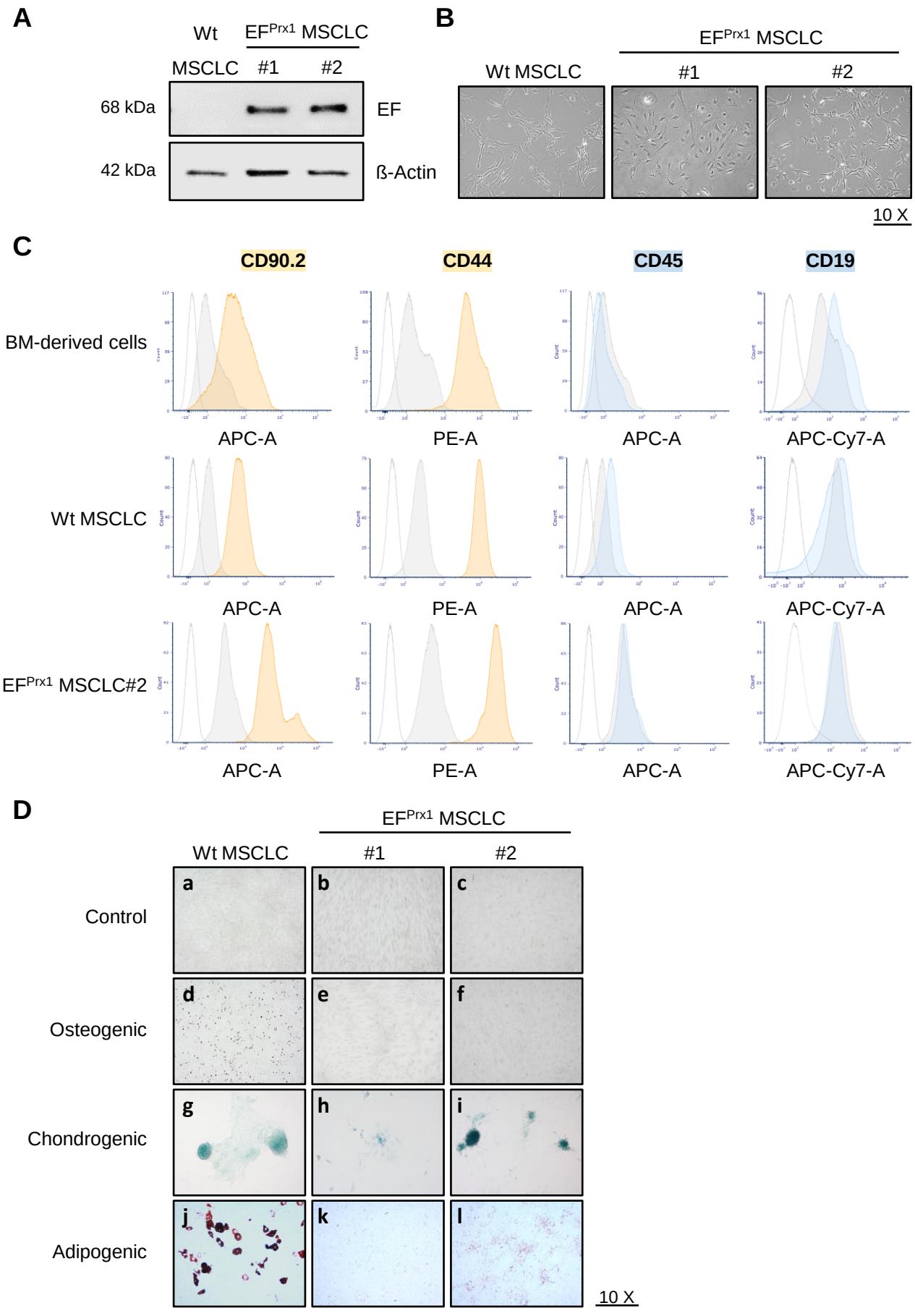
A
Wt
EFPrx1 MSCLC
MSCLC
#1
#2
68 kDa
EF
42 kDa
ß-Actin
B
EFPrx1 MSCLC
Wt MSCLC
#1
#2
10 X
C
CD90.2
CD44
CD45
CD19
BM-derived cells
Wt MSCLC
EFPrx1 MSCLC#2
APC-A
PE-A
APC-Cy7-A
D
EFPrx1 MSCLC
Wt MSCLC
#1
#2
Control
Osteogenic
Chondrogenic
Adipogenic
a
b
c
d
e
f
g
h
i
j
k
l
10 X

Figure S2. Differentiation potential of EF expressing bone derived MSCLC. EF^{Prx1} MSCLCs stably expressed EF protein and were morphologically and immunophenotypically similar to Wt MSCLC.

(A) Presence of EF protein in MSCLC isolated from EF^{Prx1} limb bud (EF^{Prx1} MSCLC) was verified with Western blot analysis using an antibody against the FLI1 C-terminus. MSCLC from the limb of Prx1Cre mice (Wt MSCLCs) served as a negative control. β-Actin was used as a loading control. **(B)** Morphology of Wt and EF^{Prx1} MSCLC#1 and #2 (magnification 10×). **(C)** Flow cytometric characterization of Wt MSCLC and EF^{Prx1} MSCLC revealing positivity for mesenchymal markers CD90 and CD44 (orang-filled peaks) and negativity for hematopoietic markers CD45 and CD19 (blue-filled peaks). Grey-filled peaks show staining with isotype controls; empty peaks show negative controls of unstained cells. **(D)** In vitro differentiation potential of MSCLC and EF^{Prx1} MSCLC#1 and #2 upon 21 days incubation with differentiation inducing cocktails for osteogenic, chondrogenic, and adipogenic differentiation. (a–f) Alizarin red staining, (g–i) Alcian blue staining, and (j–l) Oil Red O staining was used to assess osteogenic, chondrogenic, and adipogenic differentiation, respectively (magnification 10×).

Figure S3

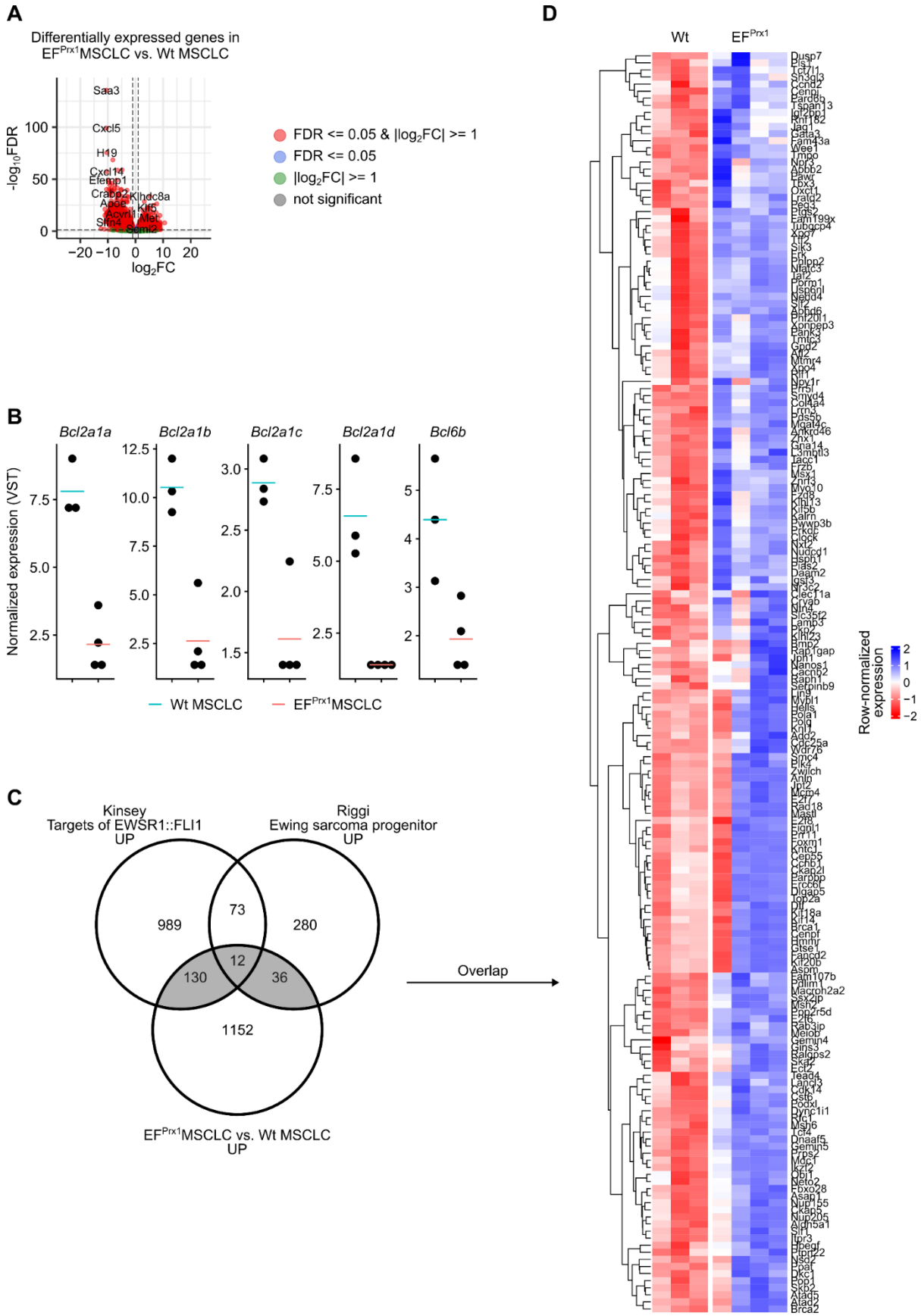
A
Differentially expressed genes in EF^Prx1 MSCLC vs. Wt MSCLC
-log10FDR
log2FC
Saa3
Cxcl5
H19
Cxcl14
Efemp1
Crabp2
Klhdc8a
Apoe
Klf5
Acvrl1
Met
Slfn4
Sema3a
FDR <= 0.05 & |log2FC| >= 1
FDR <= 0.05
|log2FC| >= 1
not significant
B
Bcl2a1a
Bcl2a1b
Bcl2a1c
Bcl2a1d
Bcl6b
Normalized expression (VST)
Wt MSCLC
EF^Prx1 MSCLC
C
Kinsey
Targets of EWSR1::FLI1
UP
Riggi
Ewing sarcoma progenitor
UP
989
73
280
12
130
36
1152
EF^Prx1 MSCLC vs. Wt MSCLC
UP
Overlap
D
Wt
EF^Prx1
Row-normalized expression
2
1
0
−1
−2

Figure S3. Differentially expressed genes between EF^{Prx1} MSCLC and Wt MSCLC.

(A) Volcano plot of differentially expressed genes between EF^{Prx1} MSCLC and Wt MSCLC identified by DEseq2. The X-axis indicates the logarithms of the fold changes of individual genes. The Y-axis indicates the negative logarithm of their P-value to base 10 (DESeq2 [S1]; $P_{adj}<0.05$, $|log2FC|>log2(2)$; n(EFPrx1) = 4, n(Wt) = 3). See **Table S2**. **(B)** Normalized RNA-seq counts of transcripts for Bcl2a family members in EF^{Prx1} MSCLC vs. Wt MSCLC groups. **(C)** Venn diagrams showing the overlap between up-regulated genes in EF^{Prx1} MSCLC vs Wt MSCLC and genes modulated by EF upon knockdown in EwS cell lines TC71 and EWS502 [S2], and genes upregulated in human mesenchymal stem cells engineered to express ectopic EF [S3]. Overlaps between human and mouse gene signatures were determined by matching gene symbols. See Table S3 for results of overlap enrichment analyses. **(D)** Heatmap showing z-score of DEseq2 normalized counts for candidate EF target in the overlap of gene signatures shown in **C**.

Figure S4

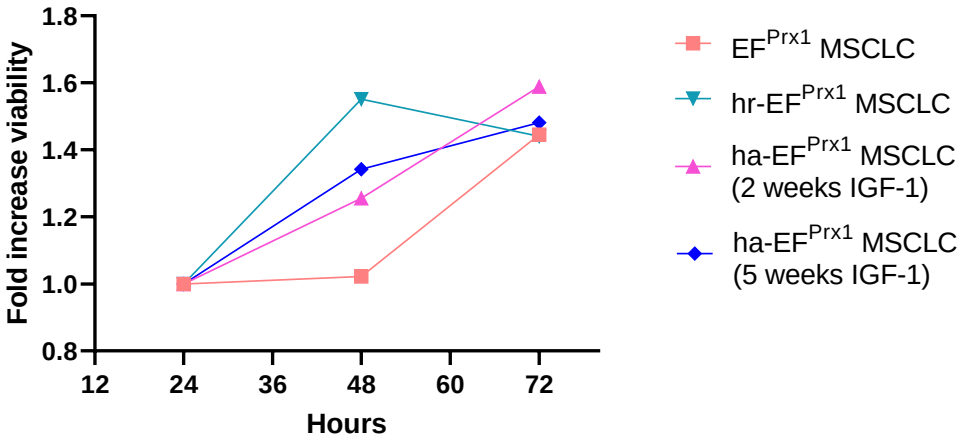

Figure S4. Increased viability of EF^{Prx1} MSCLC upon IGF-1 activation and reprogramming.

Cell proliferation differences between parental and hormone activated/reprogrammed cells were assessed using the CellTiter-Glo luminescent cell viability assay. Graph showing fold change of luminescence values, with background subtracted and normalized to the 24-hour time point to account for seeding differences. Each point represents the mean from three technical replicates.

Figure S5

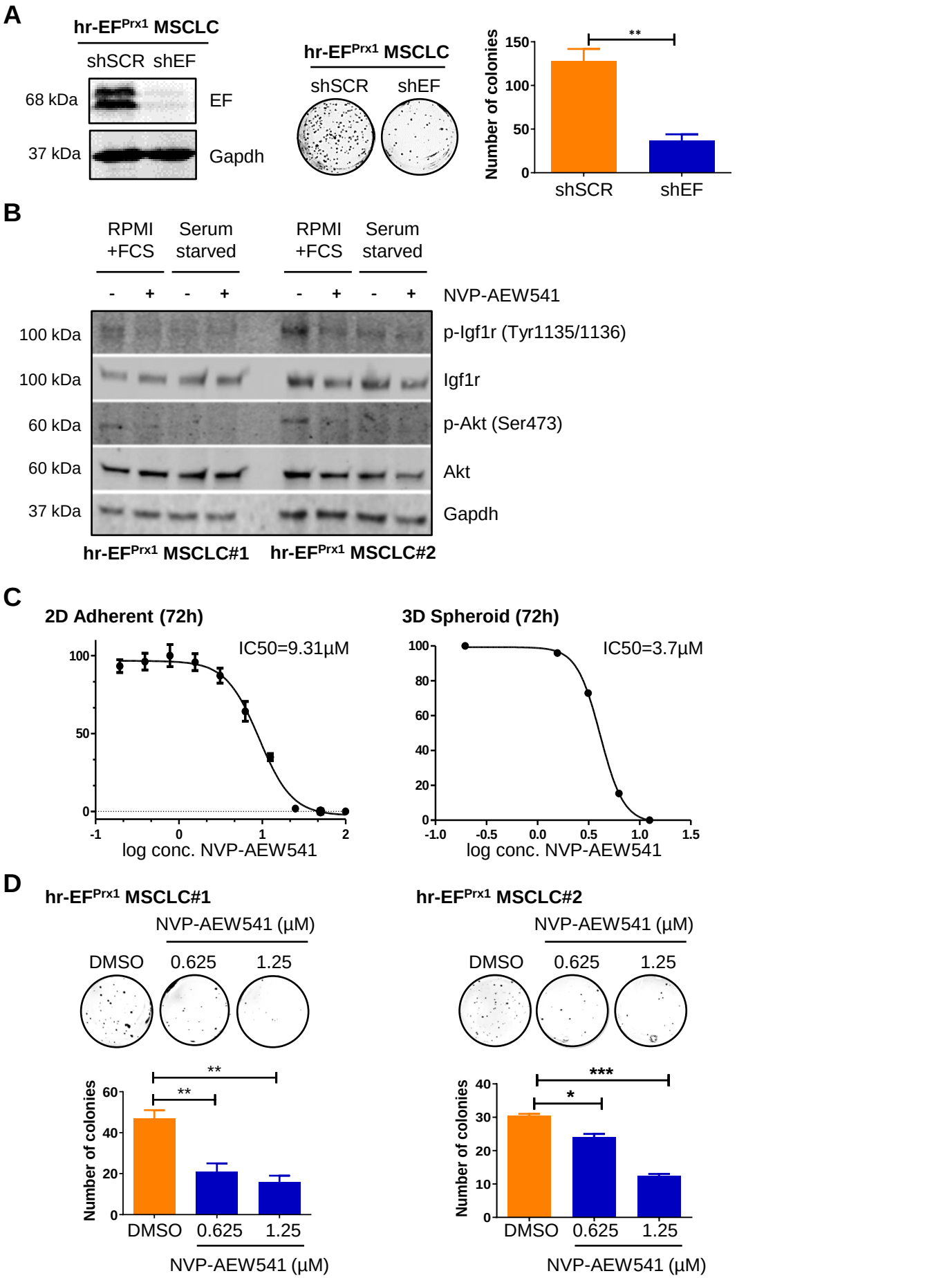
A
hr-EF^Prx1 MSCLC
shSCR shEF
68 kDa
EF
37 kDa
Gapdh
hr-EF^Prx1 MSCLC
shSCR
shEF
Number of colonies
150
100
50
0
**
shSCR
shEF
B
RPMI +FCS
Serum starved
RPMI +FCS
Serum starved
- + - + - + - +
NVP-AEW541
100 kDa
p-Igf1r (Tyr1135/1136)
100 kDa
Igf1r
60 kDa
p-Akt (Ser473)
60 kDa
Akt
37 kDa
Gapdh
hr-EF^Prx1 MSCLC#1
hr-EF^Prx1 MSCLC#2
C
2D Adherent (72h)
IC50=9.31µM
log conc. NVP-AEW541
3D Spheroid (72h)
IC50=3.7µM
log conc. NVP-AEW541
D
hr-EF^Prx1 MSCLC#1
NVP-AEW541 (µM)
DMSO
0.625
1.25
Number of colonies
**
**
DMSO
0.625
1.25
NVP-AEW541 (µM)
hr-EF^Prx1 MSCLC#2
NVP-AEW541 (µM)
DMSO
0.625
1.25
Number of colonies
***
*
DMSO
0.625
1.25
NVP-AEW541 (µM)

Figure S5. Sustained hr-EF^{Prx1} MSCLC growth depends on EF and paracrine IGF-1 expression.

(A) Dependence of hr-EF^{Prx1} MSCLC on continuous EF expression. Left: Western blot analysis of EF knockdown efficacy in hr-EF^{Prx1} cells using EF specific shRNA (sh-EF). Scrambled shRNA was used as a non-targeting control (sh-scr). Middle: representative images of soft agar colony assay for cells transduced with the indicated shRNAs. Right: Quantification of soft agar colonies. Statistics were calculated by two-sided, unpaired Student's t-test. **(B)** IGF-1R and Akt phosphorylation status of hr-EF^{Prx1} MSCLC propagated in growth medium supplemented with 10%FCS or serum-starved for 5 hours, followed by treatment with the IGF-1R inhibitor NVP-AEW541 for 2 hours at 1µM (compared to non-treated control). **(C)** Determination of IC50 values for NVP-AEW541 on hr-EF^{Prx1} MSCLCs in both 2D and 3D (spheroid) formats. **(D)** Representative pictures and quantification of soft agar colony formation of hr-EF^{Prx1} cells after 12 days incubation in absence (DMSO) or presence of NVP-AEW541 with inhibitor replenishment every 3 days. Colonies > 0.5 mm were counted using ImageJ software. Data are expressed as mean +/- SD. from three independent experiments, two-way Anova was used to determine statistical significance (*P<0.05, **P<0.01).

Figure S6

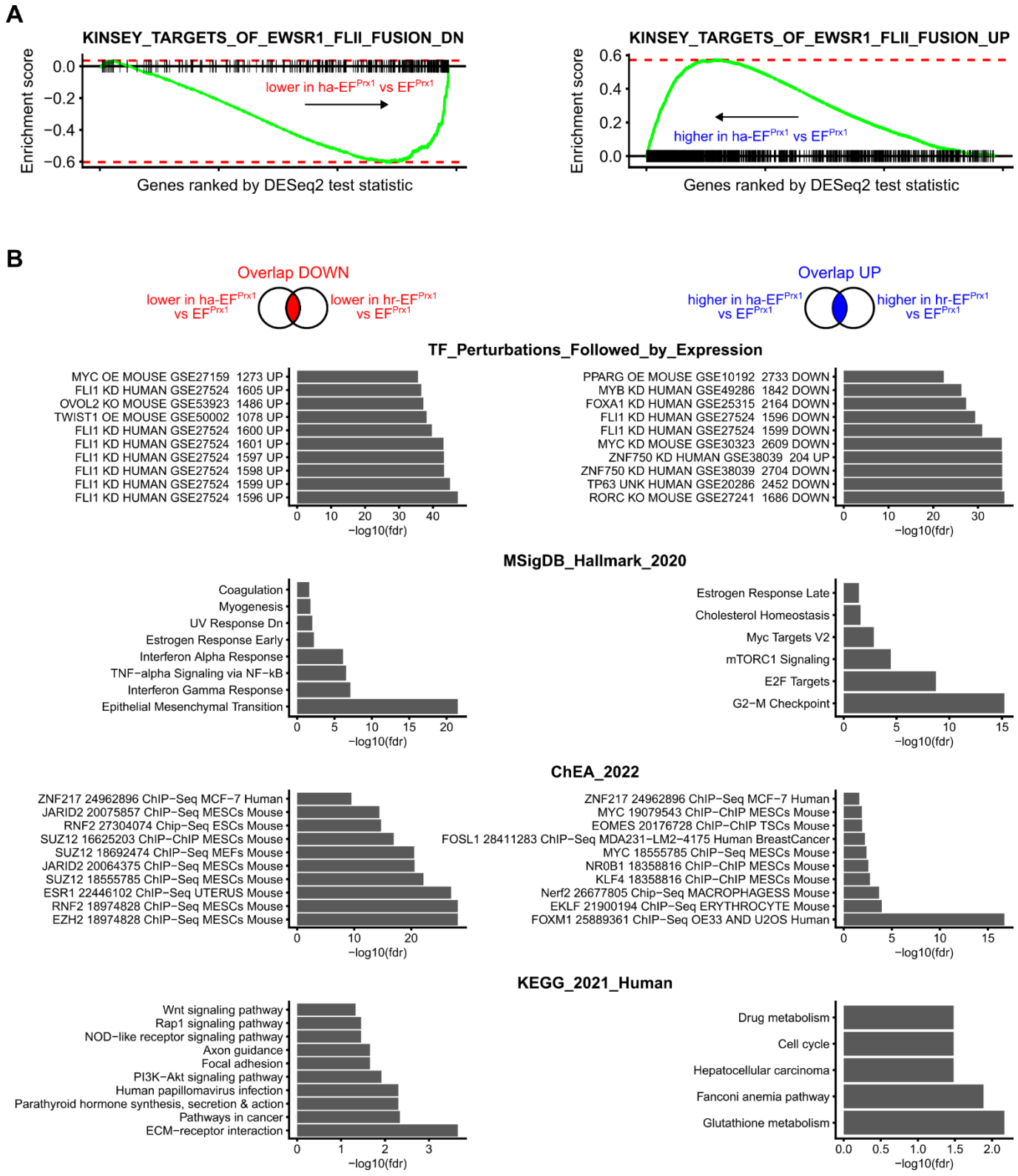
A
KINSEY_TARGETS_OF_EWSR1_FLII_FUSION_DN
Enrichment score
0.0
−0.2
−0.4
−0.6
lower in ha-EF^Prx1 vs EF^Prx1
Genes ranked by DESeq2 test statistic
KINSEY_TARGETS_OF_EWSR1_FLII_FUSION_UP
Enrichment score
0.6
0.4
0.2
0.0
higher in ha-EF^Prx1 vs EF^Prx1
Genes ranked by DESeq2 test statistic
B
Overlap DOWN
lower in ha-EF^Prx1 vs EF^Prx1
lower in hr-EF^Prx1 vs EF^Prx1
Overlap UP
higher in ha-EF^Prx1 vs EF^Prx1
higher in hr-EF^Prx1 vs EF^Prx1
TF_Perturbations_Followed_by_Expression
MYC OE MOUSE GSE27159 1273 UP
FLI1 KD HUMAN GSE27524 1605 UP
OVOL2 KO MOUSE GSE53923 1486 UP
TWIST1 OE MOUSE GSE50002 1078 UP
FLI1 KD HUMAN GSE27524 1600 UP
FLI1 KD HUMAN GSE27524 1601 UP
FLI1 KD HUMAN GSE27524 1597 UP
FLI1 KD HUMAN GSE27524 1598 UP
FLI1 KD HUMAN GSE27524 1599 UP
FLI1 KD HUMAN GSE27524 1596 UP
0 10 20 30 40
−log10(fdr)
PPARG OE MOUSE GSE10192 2733 DOWN
MYB KD HUMAN GSE49286 1842 DOWN
FOXA1 KD HUMAN GSE25315 2164 DOWN
FLI1 KD HUMAN GSE27524 1596 DOWN
FLI1 KD HUMAN GSE27524 1599 DOWN
MYC KD MOUSE GSE30323 2609 DOWN
ZNF750 KD HUMAN GSE38039 204 UP
ZNF750 KD HUMAN GSE38039 2704 DOWN
TP63 UNK HUMAN GSE20286 2452 DOWN
RORC KO MOUSE GSE27241 1686 DOWN
0 10 20 30
−log10(fdr)
MSigDB_Hallmark_2020
Coagulation
Myogenesis
UV Response Dn
Estrogen Response Early
Interferon Alpha Response
TNF−alpha Signaling via NF−kB
Interferon Gamma Response
Epithelial Mesenchymal Transition
0 5 10 15 20
−log10(fdr)
Estrogen Response Late
Cholesterol Homeostasis
Myc Targets V2
mTORC1 Signaling
E2F Targets
G2−M Checkpoint
0 5 10 15
−log10(fdr)
ChEA_2022
ZNF217 24962896 ChIP−Seq MCF−7 Human
JARID2 20075857 ChIP−Seq MESCs Mouse
RNF2 27304074 Chip−Seq ESCs Mouse
SUZ12 16625203 ChIP−ChIP MESCs Mouse
SUZ12 18692474 ChIP−Seq MEFs Mouse
JARID2 20064375 ChIP−Seq MESCs Mouse
SUZ12 18555785 ChIP−Seq MESCs Mouse
ESR1 22446102 ChIP−Seq UTERUS Mouse
RNF2 18974828 ChIP−Seq MESCs Mouse
EZH2 18974828 ChIP−Seq MESCs Mouse
0 10 20
−log10(fdr)
ZNF217 24962896 ChIP−Seq MCF−7 Human
MYC 19079543 ChIP−ChIP MESCs Mouse
EOMES 20176728 ChIP−ChIP TSCs Mouse
FOSL1 28411283 ChIP−Seq MDA231−LM2−4175 Human BreastCancer
MYC 18555785 ChIP−Seq MESCs Mouse
NR0B1 18358816 ChIP−ChIP MESCs Mouse
KLF4 18358816 ChIP−ChIP MESCs Mouse
Nerf2 26677805 Chip−Seq MACROPHAGESS Mouse
EKLF 21900194 ChIP−Seq ERYTHROCYTE Mouse
FOXM1 25889361 ChIP−Seq OE33 AND U2OS Human
0 5 10 15
−log10(fdr)
KEGG_2021_Human
Wnt signaling pathway
Rap1 signaling pathway
NOD−like receptor signaling pathway
Axon guidance
Focal adhesion
PI3K−Akt signaling pathway
Human papillomavirus infection
Parathyroid hormone synthesis, secretion & action
Pathways in cancer
ECM−receptor interaction
0 1 2 3
−log10(fdr)
Drug metabolism
Cell cycle
Hepatocellular carcinoma
Fanconi anemia pathway
Glutathione metabolism
0.0 0.5 1.0 1.5 2.0
−log10(fdr)

Figure S6. IGF-1 activation and reprogramming enforces an EWS::FLI1 transcriptional signature.

(A) Fast gene set enrichment analysis (fGSEA [S4]) of genes down/up-regulated in ha-EF^{Prx1} MSCLCs versus genes down- and up-regulated by the EWS::FLI1 fusion [S2]. Genes were pre-ranked by the DESeq2 test statistic for the comparison of ha-EF^{Prx1} MSCLC vs. EF^{Prx1} MSCLCs. **(B)** Plots showing functional gene annotations overrepresented among down-regulated (left) and up-regulated (right) genes in ha-/hr--EF^{Prx1} MSCLCs (overlaps from **Fig. 4B**). Each plot panel lists the top 10 terms (ranked by number of overlapping genes) and each bar shows the negative logarithm of the FDR-corrected P-value. Only significant enrichments are shown (P_{adj} <= 0.05). Enrichment was calculated using hypeR [S5]. See Table S8.

Figure S7

A

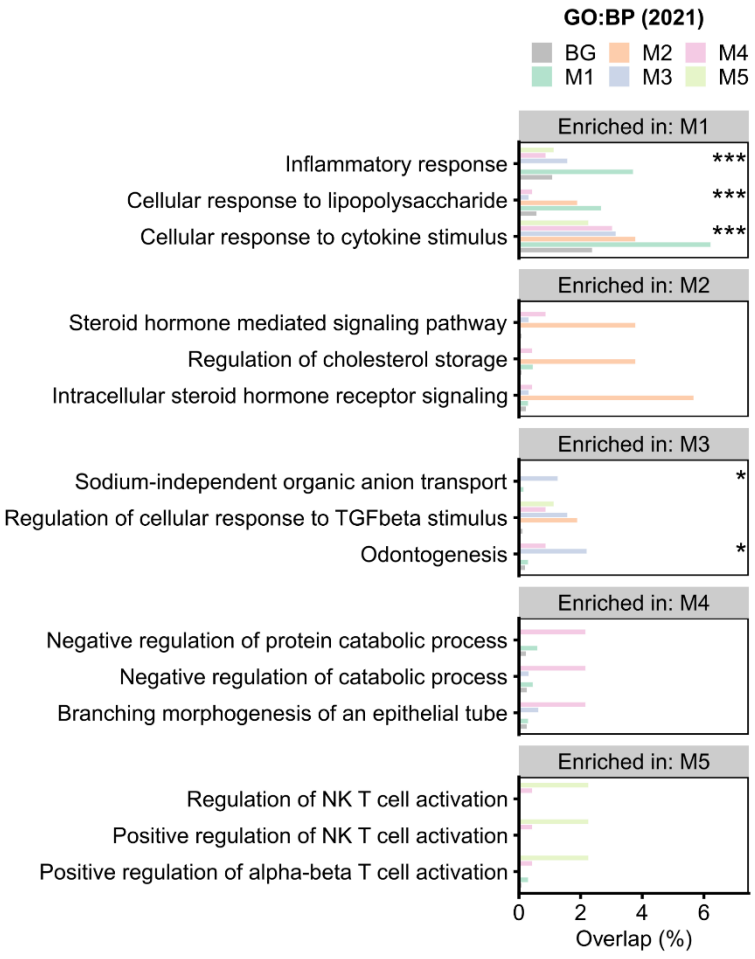

B

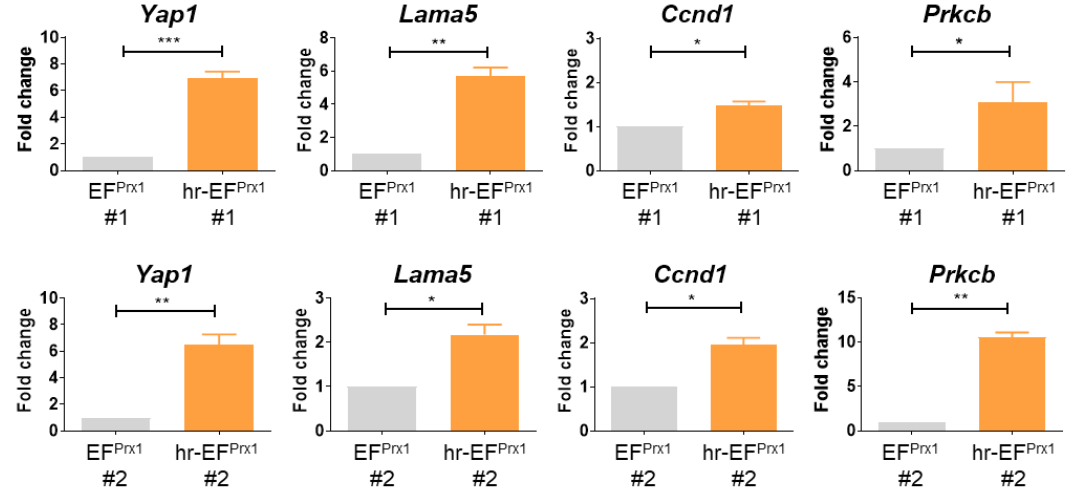

C

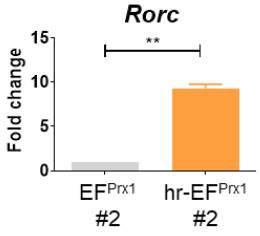

Figure S7. Characterization of chromatin cluster module M2.

(A) Plots showing gene ontology (biological process) terms overrepresented for genes associated with peaks (nearest gene) belonging to each of the five chromatin accessibility clusters displayed in **Figure 5A**. Each plot panel lists the top 3 terms per module, and each bar indicates the percentage of peaks with at least one match to the given term. Enrichment was calculated using hypeR [S5]. *, Padj < 0.05; **, P_{adj} <= 0.01; ***, P_{adj} <= 0.005. See **Table S9**. **(B)** Gene expression changes of genes linked to chromatin cluster module M2. Quantitative analysis by RT-qPCR of relative mRNA expression levels of (from left to right) Yap1, Lama5, Prkcb, and Ccnd1 in hr-EF^{Prx1} MSCLC versus EF^{Prx1} MSCLC. Statistics were calculated by one-sided, paired Student's t-test. Data is presented as mean ± SE (n = 3), ***P<0.001 **P<0.005. *P<0.01. (**C**) Quantitative analysis by measuring the relative mRNA expression levels of RorC for parental and hr-EF^{Prx1} MSCLC#1 and #2. Statistics were calculated by one-sided, paired Student's t-test. Data is presented as mean ± SE (n = 3), **P<0.005.

Figure S8

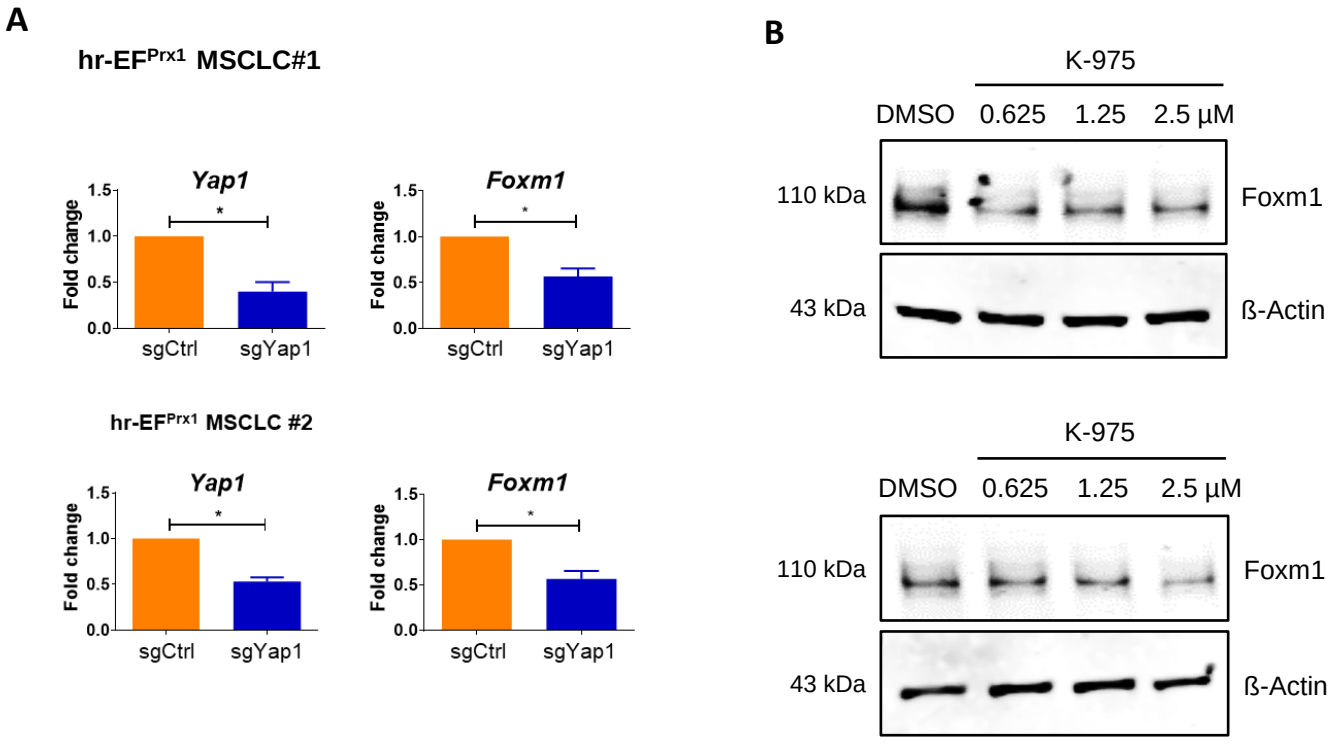

Figure S8 Yap1 knockdown results in diminished FoxM1 expression.

(A) Quantitative analysis of Yap1 expression by RT-qPCR upon sgRNA mediated knockout of Yap1. *Statistics were calculated by one-sided, paired Student's t-test. Data is presented as mean ± SE (n = 3),* * <0.05. **(B)** Immunoblot analysis of FoxM1 expression in hr-EF^{Prx1} MSCLC#2 upon treatment with increasing concentrations of the Tead palmitoylation pocket inhibitor K-975 for 24 hr.

Figure S9

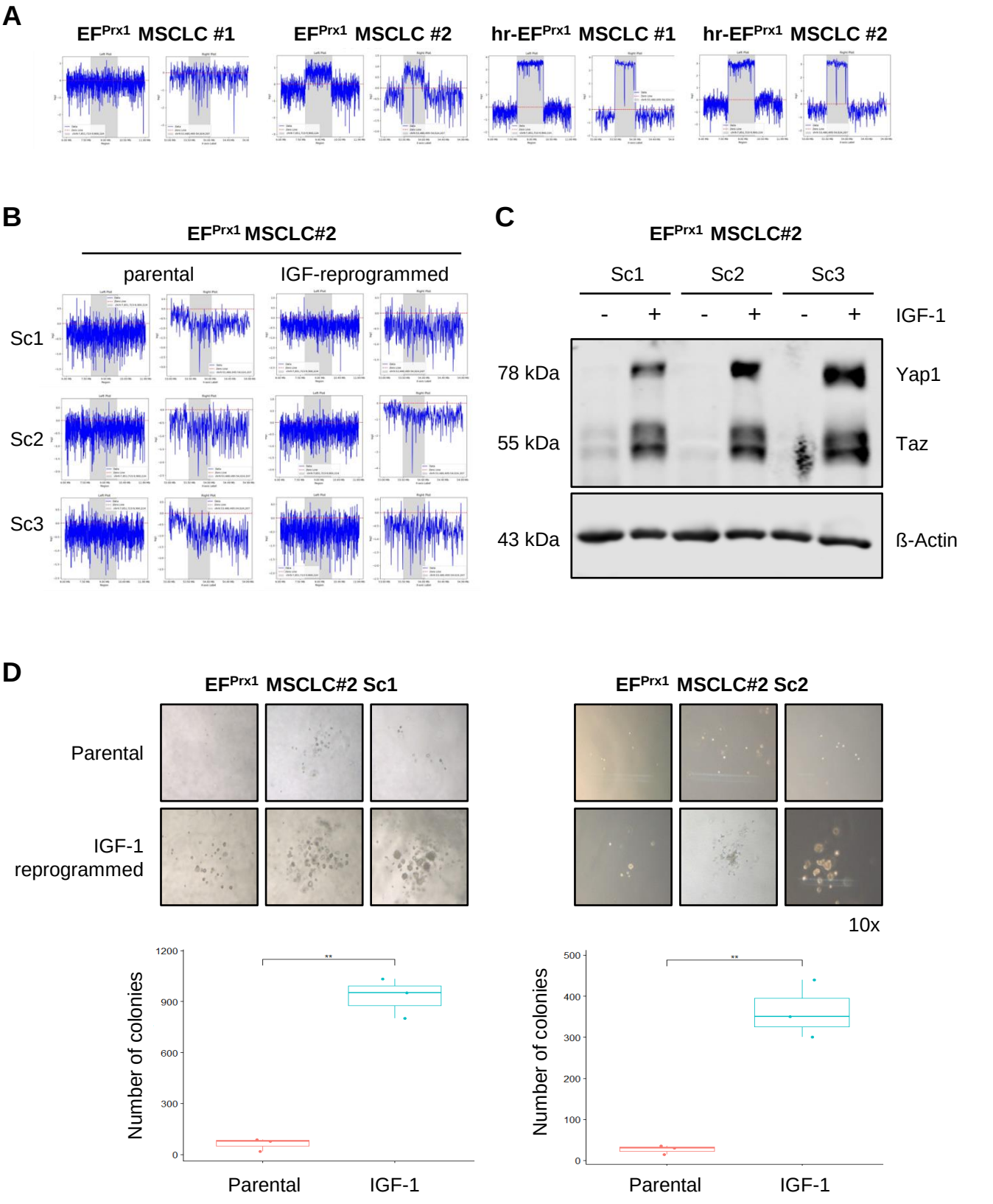
A
EFPrx1 MSCLC #1
EFPrx1 MSCLC #2
hr-EFPrx1 MSCLC #1
hr-EFPrx1 MSCLC #2
B
EFPrx1 MSCLC#2
parental
IGF-reprogrammed
Sc1
Sc2
Sc3
C
EFPrx1 MSCLC#2
Sc1
Sc2
Sc3
- + - + - +
IGF-1
78 kDa
Yap1
55 kDa
Taz
43 kDa
ß-Actin
D
EFPrx1 MSCLC#2 Sc1
EFPrx1 MSCLC#2 Sc2
Parental
IGF-1 reprogrammed
10x
Number of colonies
1200
900
600
300
0
**
Parental
IGF-1
Number of colonies
500
400
300
200
100
0
**
Parental
IGF-1

Figure S9 Yap1 induction in IGF-1 reprogrammed cells is independent of but supported by sub-clonal copy number gains at chromosome 9q.

(A) LcWGS profiles of chromosome 9q regions chr9:7,851,723-9,900,224 (left) and chr9:53,480,495-54,024,207 (right) (grey shaded areas) for bulk parental and IGF-1 reprogrammed derivative EF^{Prx1} MSCLC pools #1 and #2 identifying subtle copy number gains at the Yap1 locus (less than two-fold) in the pool derived from EF^{Prx1} founder mouse #2 but not #1 suggesting the presence of a *Yap1* amplified subclone in at least one of the parental cell lines, while derivative IGF-1 reprogrammed cell pools showed a two- to four-fold (hr-EF^{Prx1} #2) and an approximately 8-fold (hr-EF^{Prx1} #1) copy number increase at the *Yap1* locus, respectively. **(B)** To exclude IGF-1 mediated selection of a small *Yap1* amplified subclone in parental EF^{Prx1} MSCLC as the origin of stably transformed Yap1 overexpressing cells, bulk parental EF^{Prx1} MSCLC #2 were subjected to minimal dilution to raise single-cell clones followed by IGF-1 reprograming. None of three tested parental and IGF-1 reprogramed single-cell clones (Sc1, Sc2, Sc3) showed chromosome 9 copy number gains. Log2-fold copy number change (y-axis) is presented at two scales for each condition (left and right plots). **(C)** Immuno-blot analysis of Yap1, Taz, and beta actin protein expression in untreated and IGF-1 reprogrammed single-cell clones Sc1-3 derived from parental EF^{Prx1} MSCLC#2 identifying stable induction of Yap1 and to a lesser extent Taz protein expression. **(D)** Soft-agar colony formation of parental and hr-EF^{Prx1} single cell clones Sc1 and Sc2 showing a significant increase in soft agar colony formation of hr-EF^{Prx1} single cell clones lacking Yap1 amplification similar to the bulk population.

Supplemental references

[S1] Love, M.I., Huber, W., and Anders, S. (2014). Moderated estimation of fold change and dispersion for RNA-seq data with DESeq2. Genome Biol 15, 550. 10.1186/s13059-014-0550-8.

[S2] Kinsey, M., Smith, R., and Lessnick, S.L. (2006). NR0B1 is required for the oncogenic phenotype mediated by EWS/FLI in Ewing's sarcoma. Mol Cancer Res 4, 851-859. 10.1158/1541-7786.MCR-06-0090.

[S3] Riggi, N., Suva, M.L., Suva, D., Cironi, L., Provero, P., Tercier, S., Joseph, J.M., Stehle, J.C., Baumer, K., Kindler, V., and Stamenkovic, I. (2008). EWS-FLI-1 expression triggers a Ewing's sarcoma initiation program in primary human mesenchymal stem cells. Cancer research 68, 2176-2185. 10.1158/0008-5472.CAN-07-1761

[S4] Korotkevich, G., Sukhov, V., Budin, N., Shpak, B., Artyomov, M.N., and Sergushichev, A. (2021). Fast gene set enrichment analysis. bioRxiv, 060012. 10.1101/060012.

[S5] Federico, A., and Monti, S. (2020). hypeR: an R package for geneset enrichment workflows. Bioinformatics 36, 1307-1308. 10.1093/bioinformatics/btz700.